3-29-2022

The Effect of Pre-Thermal and -Load Conditions on IN-718 High Temperature Fatigue Life

Paulina De La Torre
Embry-Riddle Aeronautical University, delatop1@my.erau.edu

Alberto Mello
Embry-Riddle Aeronautical University, melloa2@erau.edu

Scholarly Commons Citation

De La Torre, P.E. and Mello, A.W. (2022) The Effect of Pre-Thermal and -Load Conditions on IN-718 High Temperature Fatigue Life. Open Journal of Applied Sciences, 12, 406-419. https://doi.org/10.4236/ojapps.2022.123028

Scientific Research Publishing

Open Journal of Applied Sciences, 2022, 12, 406-419
https://www.scirp.org/journal/ojapps
ISSN Online: 2165-3925
ISSN Print: 2165-3917

The Effect of Pre-Thermal and -Load Conditions on IN-718 High Temperature Fatigue Life

Paulina E. De La Torre, Alberto W. Mello*

Embry-Riddle Aeronautical University, Daytona Beach, USA
Email: paulina.delatorre3@outlook.com, *melloa2@erau.edu

How to cite this paper: De La Torre, P.E. and Mello, A.W. (2022) The Effect of Pre-Thermal and -Load Conditions on IN-718 High Temperature Fatigue Life. *Open Journal of Applied Sciences*, **12**, 406-419.
https://doi.org/10.4236/ojapps.2022.123028

Received: February 27, 2022
Accepted: March 26, 2022
Published: March 29, 2022

Abstract

Ni-based superalloys are largely used in the aerospace industry as critical components for turbine engines due to their excellent mechanical properties and fatigue resistance at high temperatures. A hypothesis to explain this atypical characteristic among metals is the presence of a cross-slip mechanism. Previous work on the role of thermal activation on cubic slip has shown strain accommodation in two sets of slip planes, which resembled the activation of {100} cubic slip systems along of the octahedral slip planes {111} in Ni-based superalloys under high strain and temperature, exhibiting a more homogeneous strain distribution and less strain localization. Following those previous literature evaluations of initial conditions that can potentially activate cubic-slip planes and provide the level of accommodation and strain homogenization within the grain, this paper presents some experimental procedures and results of Ni-based superalloy (IN-718) tested at 500˚C under operational loading condition, without and after being submitted to an overload and overtemperature. The experiments have shown that a pre-condition of 1% strain at 700˚C would increase the fatigue life of the IN-718 at 500˚C by four times when compared to pristine tested samples. The present results bring up the potential of improving this material fatigue performance, opening the need to further investigate the microstructure as the precondition is applied.

Keywords

Metal Fatigue, Ni-Based Superalloys, Cube Slip, Microstructure, High Temperature

1. Introduction

The development of new components in the aerospace industry has always faced

many challenges including those related to the process of material selection. Throughout the years, such applications and demands for durable, high strength, and lightweight materials increased the need for the development of new structural materials [1]. Moreover, depending on the application, some materials are more desirable than others. This was particularly true in the engine technology within the aerospace and aviation industry where the performance of materials was limited by mechanisms of deformation, such as creep during which materials are plastically deformed as a result of stresses below the yield strength, often worsen by the exposure to high-temperature environments [2]. A need for those demands is what led to much of the scientific and technological development in the early 1900s. However, it was not until the 1930s, when a new generation of materials was introduced with superalloys, then the unfamiliar γ' phase showed significant creep strengthening characteristics, thus leading to a new era of continuous discovery and improvement of superalloys [3].

Superalloys are considered high-performance complex materials that are very resistant to oxidation and high-temperature environments [4]. These types of alloys are often classified depending on the primary material present within its matrix, which can be either nickel, iron-nickel or cobalt [5]. Although their composition tends to be slightly complex, its microstructure is considered to be simpler consisting of: "an ordered, coherent γ' precipitate based on Ni_3Al; an FCC solid solution; carbides of the type MC, M6C or M23C6 depending on the temperature and composition and other minor phases such as borides" [6].

Despite having a higher cost and being harder to develop than other metals in the industry such as aluminum or stainless steel, superalloys are not only creep resistant at higher temperatures (above 650˚C) but are also resistant to corrosion and possess high mechanical strength, making them critical components in the aerospace and aviation industry [5]. These characteristics are what make superalloys suitable for many engine components, such as combustion chamber, low-pressure turbine case, burner cans, afterburners, shafts, thrust reversers, vanes, discs, and turbine blades where the materials are expected to survive under environmental conditions of extreme temperature for extended periods of time [7]. Moreover, out of different groups of superalloys, nickel-based (Ni-based) superalloys are the most common for areas above ~500˚C, and as such, the focus in this study.

Nickel-based superalloys are a rare classification of metallic materials that have been in use since the birth of gas turbine engines in the late 1930s [8]. This type of superalloy is characterized by a combination of toughness, high-temperature resistance, and resistance to environmental corrosion [9] [10] [11]. Ni-based superalloys were developed thanks to the extensive research and advances in the past decades, which resulted in the creation of these alloys capable of tolerating extreme temperatures up to 70% of its melting point (~1200˚C), thus surpassing the melting point of most metals [12] [13]. In addition to applications in power-generated turbines in aircrafts, Ni-based superalloys can also be found in a

wide range of different applications such as rocket engines and nuclear and chemical processing plants [7].

Nowadays, Ni-based superalloys account for 40% - 50% of the total weight of an aircraft engine, with Inconel 718 accounting for ~34% of the used alloys, and are mainly located in the high temperature's sections of the combustor and turbine [12]. Moreover, through several studies, it has been found that the reason behind such desirable properties is due to deformation mechanisms in the γ' precipitate where even the yield stress (σ_{ys}) increases with temperature. As initially explained by Takeuchi & Kuramoto (1973) [14], this is likely caused by cross-slip dislocations onto cubic {100} planes with cross-slipped segments acting as locks and making continued octahedral {111}-type deformations more difficult. Therefore, when compared to the {111} system, as the resolved stress on the cube slip {100} system increases, the amount of cross slip would increase, thus strengthening the γ' phase [15] [16] [17] [18]. Moreover, since slip is activated by thermal effects, increasing temperature results in a strengthening mechanism as the concentration of the cross-slipped segments (locks) increases [6].

As previously discussed, Ni-based superalloys are widely used in engine components and many other power generation applications due to their exceptional properties at high temperatures. One of the most critical characteristics of these materials is their resistance to fatigue crack initiation at operational temperatures [9] [19] [20] [21] [22] [23]. High cycle fatigue (HCF) and low-cycle fatigue (LCF) are two main components in engine applications. HCF may appear during service due to loading vibrations, and LCF may result from the repeating loading and unloading caused by power variation in the turbine [7]. Fatigue in these types of components often results in failures caused by crack nucleation.

In metals, strain localization is considered a precursor for fatigue crack initiation [16] [17] [24] [25], and it is a very important stage during the fatigue damage of crystalline materials. This concept is based on local plastic deformation within the material producing rise to slip bands in favorable crystallographic orientations in which the critical resolved shear stress has been overcome [26] [27] [28], meaning that with every new cycle, a crack is expected to grow first at a grain-by-grain level in the micro localizations before it becomes large enough to generate higher amounts of plasticity, causing it to grow perpendicular to the loading direction as predicted in classic fracture mechanics. During that stage, intrusions and extrusions of slip bands are caused by local slip activation, which, as the cycling continues, causes forward propagation of the crack [28]. For this reason, a deep understanding of the deformation factors of Ni-based superalloys is important, especially when being exposed to cyclic loading at high-temperature environments [17] [29] [30]. In the effort by Mello *et al.* (2017) [17], working with the proprietary Ni-base superalloy RR1000, the authors reported that "when submitted to high temperature and high strain (700˚C & 1%), both cubic and octahedral slip systems are activated in grains, allowing a well-distributed strain accommodation within favorably oriented grains and resulting in strain

localization within distinct regions of the microstructure". Even explaining that the γ matrix may have been alternating slip along the {111} planes as presented by Bettge and Österle (1999) yet, from mesoscale, it resembles the slip following the {100} planes [31]. Then the γ' precipitate is sheared about the {100} planes. By performing experiments SEM-DIC, they could quantify the strain accommodated by both sets of slip planes, {111} and {100}, as a function of temperature. Mello *et al.* (2017) also claimed that "if temperature is reduced to intermediate values or macroscopic strain is reduced to a value below the nominal yield strain, the material will exhibit a more homogeneous strain distribution and less strain localization, probably leading to an increase in fatigue life" [17].

In the present study, the goal is to determine with fatigue experiments if specific initial conditions will improve the fatigue life of IN-718 samples through the cube-slip activation. The chosen initial condition was based on the failure mechanism provided by Mello *et al.* (2017) [17] while studying the proprietary Ni-based superalloy RR1000. Still noted that the IN-718 contains the same level of precipitates γ' and γ'' [32], and that slip in IN-718 may not operate in the same manner as previously researched with RR1000 by Mello *et al.* (2017) [17]. The current work will solely examine the role of initial overload associated with over temperatures (T greater than T-operational) on the durability of IN-718 superalloy subjected to cyclic load and high temperature (T-operational). The study aims to examine if the precondition will improve the endurance of the material subjected to operational loading. The relationship between initial loading/temperature and the deformation mechanism may cause a direct impact on the material response under cyclic loading.

2. Methodology

The experimentations were done in two phases: 1) Preparation stage including material and equipment acquisition, experimental set-up and sample preparation; and 2) Experimental stage including data acquisition, stress-strain curves, monotonic testing at 700˚C, and fatigue testing at 500˚C.

2.1. Equipment

To conduct the experiments, the following set of equipment was used: Buehler Metaserv 250 Semiautomatic Twin Polisher, Pace Technologies GIGA-1200 Vibratory Polisher, Olympus Optical Microscope (5-100X), Branson Ultrasonic Cleaner, MTS Model 204.61 Servo Hydraulic System (11kip), MTS controller, ATS Series 3430 Split Furnace, ATS P-20-115 Temperature Controller (up to 1200˚C), National Instruments Data Acquisition System (DAQ), and Epsilon axial extensometer Model 3442. The specimen was clamped with M-246 Clevis Couplings and connected to 273 mm pull rod extensors to fit inside the furnace and keep distance from the hot section to the grip. The setup including the specimen installation in the MTS frame, the ATS furnace, and controller is depicted in **Figure 1**.

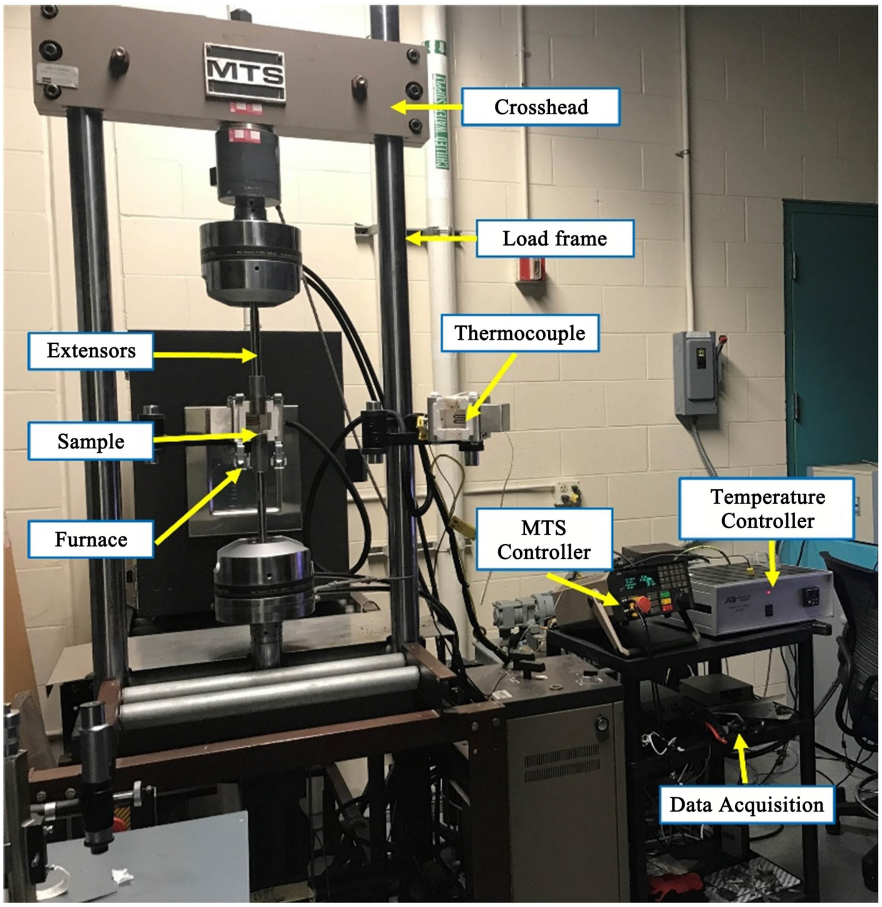

Figure 1. MTS frame and furnace system for high-temperature fatigue experiments.

2.2. Material

The bulk material acquired to conduct this study was a polycrystalline Inconel 718 Ni-based superalloy block 725 mm long, 76.2 mm wide, 19 mm thick, manufactured in accordance with AMS 5596M, HT 2180-6-9717. The composition ranges and expected properties for the material are shown in Table 1. The material was used as received, with no extra solution or heat treatment.

The samples were manufactured by electro-discharge machining (EDM) out of the IN-718 block, with a gauge length of 20 mm, a gage cross-sectional area of 3 mm, and a thickness of 1.25 mm, as depicted in Figure 2.

2.3. Sample Preparation

The sample preparation consisted of removing all surface imperfections by polishing the specimens. For future analysis, if necessary to look at the sample in a scanning electron microscope (SEM) and have the microstructure characterized by electron backscatter diffraction (EBSD), it is imperative to polish the sample until a mirror-like surface is obtained. For this application, it is important to minimize the surface deformation to observe the sample microstructure [33]. Also, any form of localized stress concentration due to previous defects and scratches must be removed to guarantee that the crack nucleation will be driven

Table 1. Inconel 178 Ni-based superalloy composition and properties (AMS 5596M).

Composition		Properties	
Component	**Weight %**	Density, kg/m^3	8193.3
Ni (+Co)	50.0 - 55.0	Melting Range, ˚C	1260 - 1336
Cr	17.0 - 21.0	Young's Modulus[a], GPa	199.9
Fe	Bal.	Torsional Modulus[a], MPa	80×10^3
Nb (+Ta)	4.75 - 5.50	Poisson's Ratio[a]	0.29
Mo	2.80 - 3.30	Tensile Strength[a], MPa	1241
Ti	0.65 - 1.15	Yield Strength (0.2% offset)[a], MPa	1034
Al	0.20 - 0.80	Elongation[a], %	12
Co	1.0 max.	[a] **At room temperature.**	
C	0.08 max.		
Mn	0.35 max.		
Si	0.015 max.		
Ph	0.015 max.		
S	0.015 max.		
B	0.006 max.		
Cu	0.30 max.		

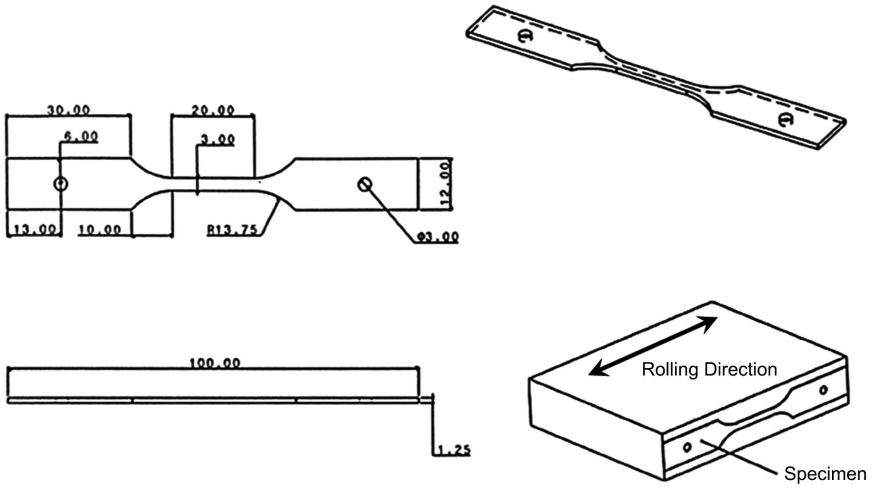

Figure 2. Manufacturing drawing of the dog-bone-shaped sample made of IN-718. All dimensions in mm.

by local strain accumulation in the microstructure, and not by an induced weakest link. Every sample was numbered for control purpose. The polishing process was performed in three stages. During the first stage, the sample was polished on a 600-grit sandpaper in conjunction with water on both sides until it became smooth to touch and all major signs of damage from the cutting process, material deformations and large deep scratches were removed. This was visually verified by using an Olympus optical microscope at a magnification of 50×. Once all

major imperfections disappeared, the second stage consisted of polishing the sample with 1200-grit sandpaper until all remaining scratches were removed. The final stage consisted of using a Pace Technologies vibratory polisher. To complete the process during this stage, NAPPAD and colloidal silica 0.05 μm were used to remove all final remaining scratches and the sample acquired a mirror-like surface. All samples were left in the vibratory polisher for 24 hours to obtain the desired finishing. To make sure the gage section was free from scratches, the side of the specimen was also polished with a hand-held rotary tool and polishing buffing wheel embedded in colloidal silica. The sample was then washed with distilled water and dried with compressed air. Then, it was deeply sonicated in acetone, followed by sonication in ethanol to remove any organic or silica residues. Figure 3 shows the stages of the sample gage section as the polish process was applied.

2.4. Experimental Procedures

This section provides a description of the experimental methodology for the high-temperature fatigue testing and verification of the applied pre-condition.

Initially, a calibration of the MTS cross-head displacement was performed with the use of an Epsilon extensometer model 3442, at room temperature. In sequence, a stress-strain curve was created using Sample 1 by crossing the yield point and unloading the specimen, using the cross-head displacement as reference for axial strain. This curve is particularly important to check the calibration, by comparing expected properties for the material, such as yield stress and Young's modulus. Figure 4 shows the final stress-stain curve obtained for the material at room temperature, and a detailed image of the linear segment for computation of the Young's modulus. The obtained values for yield stress and Young's modulus for Sample 1 at room temperature were 1020 MPa and 198 GPa, respectively.

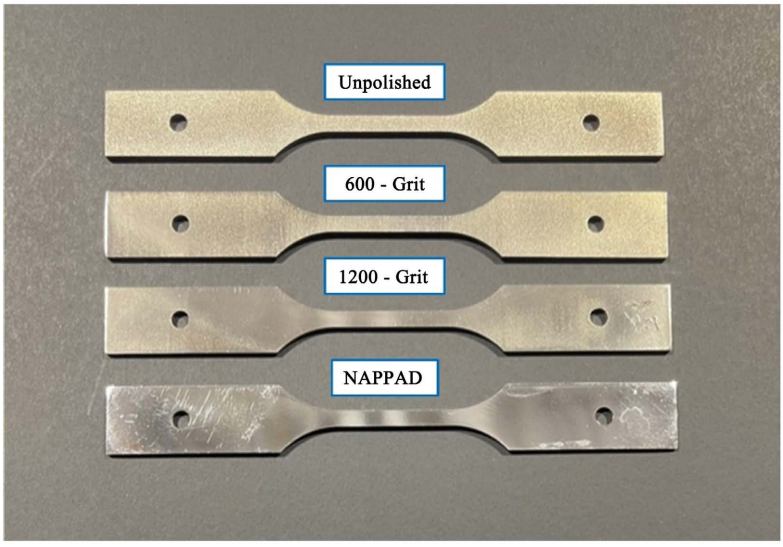

Figure 3. Samples at different polishing stages.

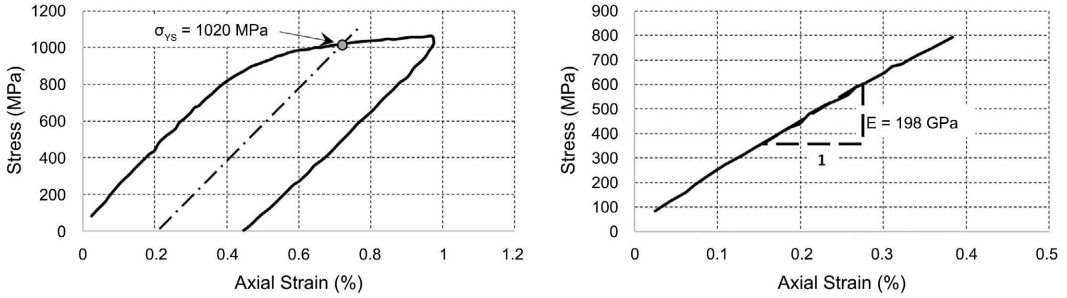

Figure 4. Stress-strain curve for IN-718 at room temperature, left: load and unload for yield stress determination, and right: zoom in the linear region for Young's modulus calculation.

In order to obtain reference stress for the high-temperature fatigue experiments, a full stress-strain curve was obtained for the highest temperature aimed during the tests (Sample 2). The procedures for the tests were as follow:

- All monotonic and fatigue experiments were performed in load control.
- Specimens were griped in the frame tester and the load was maintained at 10% of the maximum expected test load by the controller until the target temperature was achieved.
- The control thermocouple was positioned in the center of the furnace, touching the specimen gage section, to guarantee the accuracy of the temperature in the area of interest.
- Temperature was increased in small increments. For testing at 500˚C, temperature was increased by 50˚C up to 400˚C, by 10˚C up to 460˚C, and by 5˚C up to target temperature. For testing at 700˚C, temperature was increased by 50˚C up to 600˚C, by 10˚C up to 670˚C, by 5˚C up to 685˚C, and by 2˚C up to target temperature. This was done to avoid overshooting in the temperature that could cause to cross the desired temperature and possibly damage the samples.
- After the target temperature was achieved, the controller was able to maintain it within ±2%.
- Before and after each experiment, the gage section of the specimen was carefully measured to ensure the stress was accurately calculated.

Once the target temperature was achieved, the setpoint, loading rate and stress amplitude were set in the MTS controller. The stress vs. time output was graphed and cycles counted via DAQ in a LabVIEW 2016 in-house developed code.

3. Results and Discussion

High-Temperature Stress-Strain Curve

During the calibration process, the room temperature yield stress and Young's modulus for the tested specimen (Sample 1) were determined to be 1020 MPa and 198 GPa, respectively, which are in agreement with AMS 5596M. The next step was to obtain the stress-strain curve at the highest target temperature (700˚C), as shown in Figure 5. This test (Sample 2) provided yield stress and

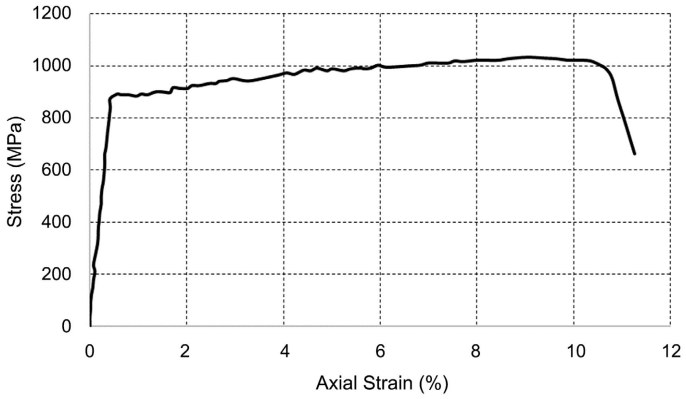

Figure 5. Stress-Strain curve for IN-718 at 700˚C.

ultimate stress of 867 MPa and 1033 MPa, respectively, and Young's modulus of 193 GPa, for the specimen at 700˚C, showing the superalloy realistically keeps its property at high temperature.

3.1. Fatigue Control Test

This step consisted of performing fatigue tests at a temperature of 500˚C until failure to determine a base for the number of cycles sustained by the sample. This was considered the control test as it was used as comparison for future tests. During this stage, a few trials were attempted (with extra samples) to find the best conditions that would produce the desired results of an expected cyclic life between 10,000 and 50,000 cycles, which was believed to be long enough to obtain good results without requiring extensive high temperature operating hours in the MTS system.

Sample 3: for the first recorded fatigue sample, the maximum stress was set as 73% of yielding stress of the material based on the stress-strain curve at 700˚C, with R = 0.1, where $R = \sigma_{\min} / \sigma_{\max}$. The specimen gage section's final dimensions were determined to be: thickness of 1.19 mm and width of 2.92 mm. The imposed maximum stress was 636 MPa, with minimum stress of 64 MPa. This specimen sustained 24,729 cycles to failure, at a frequency of 0.5 Hz.

Sample 4: To confirm the results from Sample 3 and with the objective to speed up the experiment, a new test was performed with a frequency of 1.0 Hz. The fatigue test was maintained at R = 0.1, keeping the maximum stress of 636 MPa and minimum stress of 64 MPa. Sample 4 dimensions were determined to be: thickness of 1.22 mm and width of 2.92 mm, the rupture was at 28,159 cycles.

3.2. Fatigue Test with Pre-Condition

This experiment was conducted in two steps: 1) Monotonic loading at 700˚C, in order to achieve a desired pre-condition; and 2) Cyclic fatigue at 500˚C until failure.

Sample 5:

Monotonic test—This test involved the process of applying the pre-condition to the sample. The initial dimensions of this sample were: a thickness of 1.15

mm and a width of 2.87 mm. This test was performed by heating the sample to 700˚C and loading the specimen to 884 MPa, 2% above the measured yield stress, corresponding to 1% strain based on the stress-strain curve at 700˚C, as shown in Figure 5. This level of stress was maintained for one minute to guarantee the total accommodation in the microstructure. Figure 6 shows the stress-time output for this experimental step. After unloading, the furnace was turned off, and the specimen was slowly cooled down to room temperature.

Fatigue test—After the sample was cooled down, a cyclic fatigue test at 500˚C was performed with the same parameters used in Sample 4. The test was conducted until failure. Since the sample had been subjected to overloading at 700˚C, the geometry of the sample changed in comparison to gage section measured before the monotonic test. The thickness and width of the sample gage section were properly measured, and the new area was calculated. The new specimen dimensions were: a thickness of 1.09 mm and a width of 2.49 mm. The final fracture occurred at 111,361 cycles, which was almost four times the fatigue life achieved by Sample 4 with similar loading conditions, but without the pre-overloading and pre-thermal conditions. Table 2 summarizes the results from the static and fatigue tests performed in this effort.

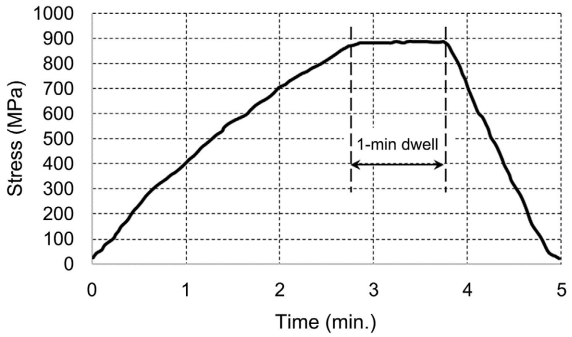

Figure 6. Monotonic loading up to 884 MPa (1% strain) at 700˚C, with 1-min. dwell time.

Table 2. Summary of the static and fatigue experiments on IN-718, AMS 5596M.

Monotonic Tests					
Sample	**Temperature**	σ_{ys}	σ_{ult}		***E***
1	Room	1020 MPa	N/A		198 GPa
2	700˚C	867 MPa	1033 MPa		193 GPa
Pre-Loading and Fatigue Tests					
Sample	**Temperature**	σ_{max}	σ_{min}	**Frequency**	**Cycles**
3	500˚C	636 MPa	64 MPa	0.5 Hz	24,729*
4	500˚C	636 MPa	64 MPa	1.0 Hz	28,159*
5	700˚C	884 MPa	0	N/A	1
	500˚C	636 MPa	64 MPa	1.0 Hz	111,361*

*Cycles to failure.

3.3. Discussion

In the present work, static and fatigue tests were performed in samples made of IN-718, AMS 5596M. The sequence and loading for these experiments were guided by previous results obtained by Mello *et al.* (2017) [17], working with proprietary Ni-based superalloy RR-1000. It is important to mention that in the cited work, the experiments were performed inside a vacuum chamber and the specimen was heated by a contact element. The test was performed at low frequency (0.15 Hz) due to limitation of the load frame. In this work, we tested the specimen in lab environment inside a mini furnace as shown in **Figure 1**, at frequency of 0.5 and 1 Hz.

The room temperature static test with the designed sample has shown that the chosen material is within the specification from AMS 5596M. The static test of the IN-718 sample at 700˚C has shown that the material retains about 85% of its yield strength, and 97% of Young's modulus at 700˚C, in comparison to the experiment at room temperature.

With the stress-strain curve at 700˚C, it was possible to determine the value of stress that corresponds to 1% strain. The value of 1% strain was chosen to match the experiment previously conducted by Mello *et al.* (2017), which showed both octahedral and cubic slip planes activations in mesoscale at 700˚C, for the RR1000. While it was uncertain in their results if the γ matrix was alternating slip along the {111} planes, some slip lines followed the {100} planes. It was hypothesized that the γ' precipitate is sheared about the {100} planes. Using their findings as reference, the value of stress corresponding to 1% strain was applied at 700˚C and maintained for a sufficient period of time to ensure full accommodation of the microstructure. The sample was then tested in fatigue at 500˚C, and the result was compared to the other two experiments conducted at 500˚C with pristine samples. The results have shown that the pre-condition applied in the specimen increased the fatigue life by approximately four times, supporting the assumption that high strain associated with high temperature may reduce the effect of strain localizations, which would increase the fatigue life under lower stress levels. The homogenization of localized strain has yet to be confirmed, however, the application of the pre-load caused a positive effect in the endurance for the studied Ni-based superalloy, under cyclic load at 500˚C.

In the next step, digital image correlation (DIC) or equivalent process could be used to measure localized strain in the area of interest to follow the slip lines at microscopic scale. Moreover, mapping of this area must be done by Electron Backscattering Diffraction (EBSD) to confirm the lattice orientations. Another important investigation would include TEM to identify if the mesoscale cubic slip plane activity, if present in IN-718, followed the zig-zag mechanism as presented by Bettge and Österle (1999) [31], or if any signs of dislocation climb is present at elevated temperatures. In addition, different levels of pre-load condition and temperature may be tested to optimize the gain in fatigue life.

4. Conclusion

Ni-based superalloy (IN-718) was tested at 500˚C under operational loading condition. The experiments were also performed in samples subjected to overload and overtemperature. The experiments have shown that a pre-condition of 1% strain at 700˚C would increase the fatigue life of the IN-718 at 500˚C by four times when compared to pristine tested samples. The present results bring up the potential of improving this material fatigue performance, opening the need to further investigate the microstructure as the precondition is applied.

Conflicts of Interest

The authors declare no conflicts of interest regarding the publication of this paper.

References

[1] Boyer, R.R., Cotton, J.D., Mohaghegh, M. and Schafrik, R.E. (2015) Materials Considerations for Aerospace Applications. *MRS Bulletin*, **40**, 1055-1066. https://doi.org/10.1557/mrs.2015.278

[2] Smith, T., Duchao, L., Hanlon, T., Wessman, A., Wang, Y., Mills, M. and Mills, M. (2016) Determination of Orientation and Alloying Effects on Creep Response and Deformation Mechanisms in Single Crystals of Ni-Base Disk Superalloys. *Superalloys* 2016: *Proceedings of the* 13*th International Symposium on Superalloys*, 579-588. https://doi.org/10.7449/Superalloys/2016/Superalloys_2016_579_588

[3] Sims, C.T. (1984) A History of Superalloy Metallurgy for Superalloy Metallurgists. Superalloys, 399-419. https://doi.org/10.7449/1984/Superalloys_1984_399_419

[4] Brooks, J.W. and Bridges, P.J. (1988) Metallurgical Stability of Inconel Alloy 718. Superalloys, 33-42. https://doi.org/10.7449/1988/Superalloys_1988_33_42

[5] Donachie, M.J., Donachie, S. and Superalloys, J. (2002) A Technical Guide. 2nd Edition, ASM International, Almere. https://doi.org/10.31399/asm.tb.stg2.9781627082679

[6] Antolovich, S.D. (2015) Microstructural Aspects of Fatigue in Ni-Base Superalloys. *Philosophical Transactions of the Royal Society A*, **373**, Article ID: 20140128. https://doi.org/10.1098/rsta.2014.0128

[7] Mouritz, A.P. (2012) Introduction to Aerospace Materials. Woodhead Publishing, Sawston. https://doi.org/10.2514/4.869198

[8] Walley, J.L. (2012) Exploration of Local Strain Accumulation in Nickle-Based Superallys. Graduate Program in Materials Science and Engineering. Ohio State University, Columbus.

[9] Gell, M., Leverant, G.R. and Wells, C.H. (1970) The Fatigue Strength of Nickel-Base Superalloys. In: *Achievement of High Fatigue Resistance in Metals and Alloys*, ASM International, Almere, 113-153. https://doi.org/10.1520/STP26842S

[10] Garimella, L., Liaw, P.K. and Klarstron, D.L. (1997) Fatigue Behaviour in Nickel-Based Superalloys: A Literature Review. *JOM*, **49**, Article No. 67. https://doi.org/10.1007/BF02914771

[11] Furrer, D. and Fecht, H. (1999) Ni-Based Superalloys for Turbine Discs. *JOM*, **51**, 14-17. https://doi.org/10.1007/s11837-999-0005-y

[12] Pollock, T.M. and Tin, S. (2006) Nickel-Based Superalloys for Advanced Turbine Engines: Chemistry, Microstructure, and Properties. *Journal of Propulsion and Power*, **22**, 361-374. https://doi.org/10.2514/1.18239

[13] Deng, D. (2018) Additively Manufactured Inconel 718: Microstructures and Mechanical Properties. Linköping University, Linköping.

[14] Takeuchi, S. and Kuramoto, E. (1973) Temperature and Orientation Dependence of the Yield Stress in Ni3Ga Single Crystals. *Acta Metallurgica*, **21**, 415-425. https://doi.org/10.1016/0001-6160(73)90198-3

[15] Kalluri, S. and Mc.Gaw, M.A. (1990) Effect of Tensile Mean Stress on Fatigue Behavior of Single-Crystal and Directionally Solidified Superaolloys. Technical Memorandum, National Aeronautics and Space Administration, Washington DC, 1-21.

[16] Stinville, J.C., Epichlin, M.P., Callahan, P.G., Miller, V.M., Texier, D., Bridier, F., *et al*. (2017) Measurement of Strain Localization Resultingfrom Monotonic and Cyclic Loading at 650˚C in Nickel Base Superalloys. *Experimental Mechanics*, **57**, 1289-1309. https://doi.org/10.1007/s11340-017-0286-y

[17] Mello, A.W., Nicolas, A. and Sangid, M.D. (2017) Fatigue Strain Mapping via Digital Image Correlation for Ni-Based Superalloys: The Role of Thermal Activation on Cube Slip. *Materials Sicence & Engineering*, **695**, 332-341. https://doi.org/10.1016/j.msea.2017.04.002

[18] Deng, W., Xu, J., Hu, Y., Huang, Z. and Jiang, L. (2019) Isothermal and Thermomechanical Fatigue Behavior of Inconel 718 Superalloy. *Material Sicence & Engineering*, **742**, 813-819. https://doi.org/10.1016/j.msea.2018.11.052

[19] Antolovich, B.F. (1996) Fatigue and Fracture of Nickel-Base Superalloys. In: ASM Handbook Committee, Ed., *AMS Handbook*: *Fatigue and Fracture*, Vol. 19, ASM International, Almere, 854-868. https://doi.org/10.31399/asm.hb.v19.a0002410

[20] Kirka, M.M., Medina, F., Dehoff, R. and Okello, A. (2016) Mechanical Behavior of Post-Processed Inconel 718 Manufactured through the Electron Beam Melting Process. *Materials Science & Engineering*: *A*, **680**, 338-346. https://doi.org/10.1016/j.msea.2016.10.069

[21] Belan, J., Kuchariková, L., Tillová, E., Závodská, D. and Chalupová, M. (2018) Effect of Fatigue Loading Mode on 718 Fatigue Properties. *Periodica Polytechnica Transportation Engineering*, **47**, 335-341. https://doi.org/10.3311/PPtr.12114

[22] Kevinsanny, Okazaki, S., Takakuwa, O., Ogawa, Y., Okita, K., Funakoshi, Y., Matsunaga, H. (2019) Effect of Defects on the Fatigue Limit of Ni-Based Superalloy 718 with Different Grain Sizes. *Fatigue & Fracture of Engineering Materials & Structures*, **42**, 1203-1213. https://doi.org/10.1111/ffe.12989

[23] Jiang, R., Song, Y.D. and Reed, P.A. (2020) Fatigue Crack Growth Mechanisms in Powder Metallurgy Ni-Based Superalloys—A Review. *International Journal of Fatigue*, **141**, Article ID: 105887. https://doi.org/10.1016/j.ijfatigue.2020.105887

[24] Mello, A.W., Nicolas, A., Lebensohn, R.A. and Sangid, M.D. (2016) Effect of Microstructure on Strain Localization in a 7050 Aluminumalloy: Comparison of Experiments and Modeling for Various Textures. *Materials Science & Engineering*, **661**, 187-197. https://doi.org/10.1016/j.msea.2016.03.012

[25] Zhong, L., Hu, H., Liang, Y. and Huang, C. (2019) High Cycle Fatigue Performance of Income 718 Alloys with Different Strengths at Rooms Temperatures. *Metals*, **9**, Article No. 13. https://doi.org/10.3390/met9010013

[26] Carroll, J., Abuzaid, W., Lambros, J. and Sehitoglu, H. (2010) An Experimental Methodology to Relate Local Strain to Microstructural Texture. *Review of Scientific Instruments*, 81, Article ID: 083703. https://doi.org/10.1063/1.3474902

[27] Storgärds, E. (2015) High Temperature fatigue Crack Growth in a Ni-Based Superalloy. Linköping University, Linköping.

[28] Miao, J., Pollock, T.M. and Jones, J.W. (2008) Fatigue Crack Initiation in Nickel-based Superalloy René 88 DT at 593˚C. In: Reed. R.C., *et al*., Eds., *Superalloys* 2018, Department of Materials Science and Engineering, University of Michigan, Ann Arbor, 589-597. https://doi.org/10.7449/2008/Superalloys_2008_589_597

[29] Korth, G.E. (1980) Mean Stress Effects on High-Cycle Fatigue of Alloy 718. EG&G Idaho, Inc., Idaho Falls. https://doi.org/10.2172/5493726

[30] Ling, L.-S.-B., Yin, Z., Hu, Z., Wang, J. and Sun, B.-D. (2019) Effects of the γ"-Ni3Nb Phase on Fatigue Behavior of Nickel-Based 718 Superalloys with Different Heat Treatments. *Materials*, **12**, Article No. 3979. https://doi.org/10.3390/ma12233979

[31] Bettge, D. and Österle, W.(1999) "Cube Slip" in Near-[111] Oriented Specimens of a Single-Crystal Nickel-Base Superalloy. *Scripta Materialia*, **40**, 389-395. https://doi.org/10.1016/S1359-6462(98)00446-1

[32] Tucho, W.M., Cuvillier, P., Sjolyst-Kverneland, A. and Hansen, V. (2017) Microstructure and Hardness Studies of Inconel 718 Manufactured by Selective Laser Melting before And after Solution Heat Treatment. *Materials Science & Engineering*: *A*, **689**, 220-232. https://doi.org/10.1016/j.msea.2017.02.062

[33] Nowell, M.M., Witt, R.A. and True, B.W. (2005) EBSD Sample Preparation: Techniques, Tips, and Tricks. *Microscopy Today*, **13**, 44-49. https://doi.org/10.1017/S1551929500053669